



Lithium redistribution around the crack tip of lithium-ion battery electrodes

Le Yang^a, Hao-Sen Chen^{b,c,*}, Hanqing Jiang^d, Wei-Li Song^{b,c,*}, Daining Fang^{a,b,*}

^a China State Key Laboratory for Turbulence and Complex Systems, College of Engineering, Peking University, Beijing 100871, China

^b Beijing Key Laboratory of Lightweight Multi-functional Composite Materials and Structures, Beijing Institute of Technology, Beijing 100081, China

^c State Key Laboratory of Explosion Science and Technology, Institute of Advanced Structure Technology, Beijing Institute of Technology, Beijing 100081, China

^d School for Engineering of Matter, Transport and Energy, Arizona State University, Tempe, AZ 85287, USA

ARTICLE INFO

Article history:

Received 5 January 2019

Received in revised form 18 March 2019

Accepted 22 March 2019

Available online xxxx

Keywords:

Lithium-ion batteries

Electrochemistry

Stress-assisted diffusion

Silicon

Crack tip

ABSTRACT

Silicon film with pre-crack was used to study the coupling effect of stress and electrochemical field around the crack tip. The in-situ experiments were established to monitor the crack to realize the stress concentration around the crack and simultaneously prevent the crack initiation. The ex-situ Auger electron spectroscopy experiments shown the remarkably Li redistributed phenomenon around the crack tip. Furthermore, the fully coupled finite element method was used to reveal the fundamental mechanisms of the Li gathering effect and the stress relaxation phenomenon around the crack tip.

© 2019 Published by Elsevier Ltd on behalf of Acta Materialia Inc.

Lithium-ion batteries (LIBs), which possess high energy capacity and long cycle life, are used in many fields, such as the electric vehicles, consumer electronics and the storage system of the renewable energy [1–4]. However, for those high capacity electrode materials (Si, Sn, et al), the mechanical degradation, which result from the large deformation and fracture of the electrode during the Li insertion/desertion, would significantly limit the performance of the LIBs and impede its commercial application [5–11]. This complex diffusion induced effect has been widely studied. The in-situ experiments have been used to observe the deformation and crack evolution of the electrodes [12–15], and the critical size of the electrodes could also be determined by fracture mechanical theory under consideration of the volume expansion of electrodes during lithiation [16–20]. Except for the influence of Li insertion on the deformation of the electrodes, the stress could also affect the Li diffusion process in the electrodes, and this behavior has been qualitatively proved in the previous experiments [21–25]. This coupled effect between electrochemistry and mechanics would be more serious around the crack tip result from the stress concentration and crack evolution.

Many fully coupled theoretic and numerical methods of electrochemical fracture mechanics have been developed to analyze the fracture behavior of the electrodes. The path independent J-integral which contain the coupled term was derived to represent the driving force around the crack tip, and this constitutive relation was applied to the finite element analysis (FEA) [26–30]. The simulation results show the Li redistribution phenomenon around the crack tip, which was due to the Li diffusion under the stress gradient. Besides, the phase-field method was also used to simulate the crack initiation, propagation, and branching, this work reveals the evolution of inner and surface crack during the Li insertion and extraction, respectively, and they also studied the redistributive behavior of Li around the crack tip [31–35]. However, up to now, this Li distribution phenomenon around the crack tip of the electrodes was just found in the simulated or theoretical results [26,36], and the experimental evidence is still absent due to the difficulty of the mechanical loading and Li concentration measurement in the electrochemical environment inner the LIBs. Besides, the appropriate moment, which could ensure the stress concentration and prevent the crack initiation at the same time, was also hard to determine.

In this work, we prepared the silicon electrodes and fabricated a pre-crack on it. Then we developed the in-situ experimental methods to realize the tensile stress loading and Li redistribution around the tip. After that, the Li distribution mapping around the crack tip was quantitatively measured by the Auger electron spectroscopy (AES), and the coupled behavior of Li diffusion and stress evolution was also simulated by the all coupled FEA.

* Corresponding authors at: Beijing Key Laboratory of Lightweight Multi-functional Composite Materials and Structures, Beijing Institute of Technology, Beijing 100081, China.

E-mail addresses: chenhs@bit.edu.cn (H.-S. Chen), weilis@bit.edu.cn (W.-L. Song), fangdn@pku.edu.cn (D. Fang).

Experimentally, the 311 nm thick pure Si film electrode was prepared by the magnetron sputtering (Kurt J. Lesker LAB 18), the 500 μm thick quartz and ~ 300 nm deposited Cu were used as the substrates and the current collectors, respectively. The detail information of the preparation techniques and the characterization of the Si could be found in our previous work [37,38]. The pre-crack was manufactured by the focus ion beam (FIB, FEI Strata DB23), and the length of the crack is $2a = 20$ μm , the width is 1 μm (Fig. 1a). The Si electrodes were placed in our home-made in-situ electrochemical cell [37–39] and assembled in the argon-filled glove box (Mbraun Inc.).

As shown in Fig. 1b The special charge-discharge strategy was used to realize the maximized Li redistribution around the crack tip.

- Step 1.** In order to obtain the homogeneous Li distribution before the Li extraction, the electrode was discharged (corresponding lithiation process in half-cell) using the constant current constant voltage (CCCV) strategy, the current was 100 μA (400 $\mu\text{A cm}^{-2}$), and the cut-off voltage was 0.3 V (vs. Li/Li^+). As shown in the previous in-situ experiments and the simulation [37,38], during the Li insertion, the film only expansion along the z-direction, and there is no deformation at the x-y plane.
- Step 2.** After the discharging process, the battery was charged to 0.7 (vs. Li/Li^+) using the same current value. As shown in Fig. 1c–d, the electrode would be shrinking during Li desertion, thus the film thickness h would decrease at the z-direction, and the biaxial tensile stress would be introduced in the x-y plane by reason of the basement constrain. The tensile stresses have been measured in lots of work by multi-beam optical sensor (MOS) method [40–42]. Then, the stress concentration would occur around the pre-crack.
- Step 3.** As the response time of Li diffusion was much small than the response time of stress, this step was a rest procedure, and its long enough to ensure the open-circuit voltage of the battery become constant. Meanwhile, the Li redistribution process occurred inner the Si film, and the Li-ion will gather to the crack tip driven by the stress gradient.

The optical microscopy (Keyence Corporation) was used to monitor the electrode with a crack in the in-situ batteries, and these parameters

used in these steps were determined after multi-rounds of optimization to simultaneously guarantee the tensile stress large enough and prevent the crack initiation. In the process of optimization, many cut-off voltages lower than 0.3 V have been tried during the in-situ experiments, and the results show the film would be crack after delithiation (Fig. S1), and the AES mapping experiment could not continue on the cracked film. The cut-off charge voltage 0.7 V was determined from the MOS results [40], which will guarantee the tensile stress inner the film. If the cut-off charge voltage above 0.7 V, the tensile stress would not be guaranteed, and there will no Li redistribution around the crack tip.

The Li distribution around the crack tip was characterized by the AES (PHI700 ULVAC), the pressure in the system was less than 3.9×10^{-9} Torr, and primary electron beam energy was 10 keV. Fig. S2 shows the Auger spectra and the atomic concentration of electrodes surface and internal (after 2 min etching, 10 nm reduction reference to crystalline silicon). The results show the solid electrolyte interface (SEI) was generated at the surface of the electrode during the lithiation process, and its major chemical elements are C, Li, and F. However, after etching, the atomic concentrations of F and C element was obviously decreased, this result indicates the SEI were removed from the Li_xSi film.

Fig. 2a shows the scanning electron microscope (SEM) image of the crack tip after etching, and the quantitative AES mapping was obtained at the same area. The Li concentration distribution C was shown in Fig. 2b, and it was normalized by its average concentration C_{ave} . Due to the dramatic change of the height, the atomic concentration inner the crack (white dashed triangle) cannot reflect the actual concentration. Besides, the island-like gray/white region in the SEM image indicates the rough surface of the lithiated silicon film after etching. The previous results measured by in situ AFM (atomic force microscopy) have also find this characteristic of the thin film electrodes prepared by magnetron sputtering [43,44]. The noise points in the AES mapping results were also caused by the rough surface, however, its size is smaller than the crack tip region and has little effect on the experimental results. The Li distributions indicated distinctly Li concentrated behavior around the crack tip, and the size of involved area is around 5–10 μm . Fig. 2c shows the Li distribution along the red line in Fig. 2b, the red curve is the fitting date of the primary result and also proved the increase of the Li concentration at the crack tip. Fig. 2d shows the

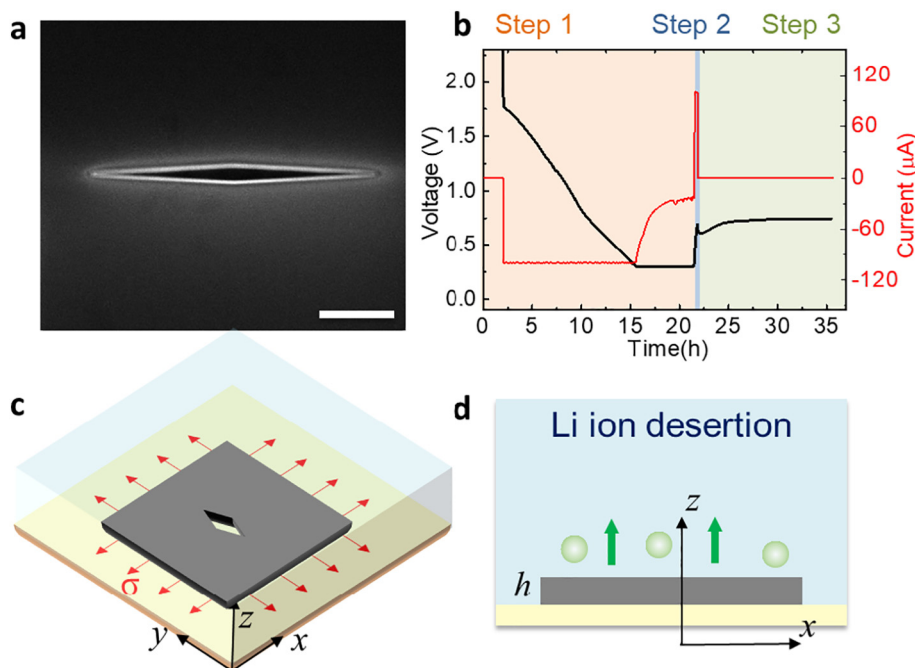


Fig. 1. (a) SEM image of the electrodes with pre-crack manufactured by FIB. (b) The charge-discharge curve of the electrodes. (c–d) Schematic diagram of the stress evolution during the Li desertion process. The scale bare is 5 μm .

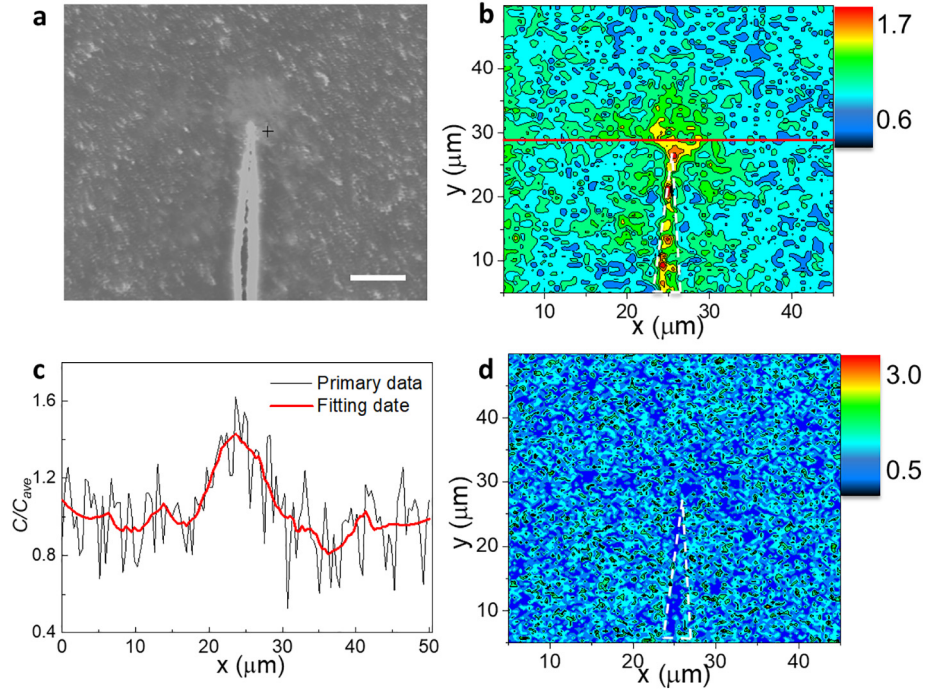


Fig. 2. (a) SEM image of the crack tip after etching. (b) Normalized Li concentration distribution around the crack tip measured by AES. (c) The normalized Li concentration along the red line in panel b. (d) Normalized Si concentration distribution around the crack tip. The scale bar is 5 μm . (For interpretation of the references to color in this figure legend, the reader is referred to the web version of this article.)

Si distribution in the electrode, which was also normalized by its average value, and have a little change around the crack.

For a deep analysis of the entire process of the interaction between the stress concentration and Li distribution around the crack tip, the fully coupled chemical mechanical finite element simulation was performed. The deformation gradient \mathbf{F} of the lithiated silicon could be decomposed into three parts, and the principal stretches could correspondingly be decomposed into elasticity, plasticity and concentration parts,

$$\lambda_i = \lambda_i^e \lambda_i^p \lambda_i^c \quad (1)$$

where $i = 1, 2, 3$, no summation convention, and the superscripts 'e', 'p' and 'c' denote elastic, plastic and concentration parts, respectively.

The constitutive relationship with the effect of diffusion-induced deformation and the chemical potential including stress can be expressed as

$$\sigma_i = \frac{1}{\lambda_1 \lambda_2 \lambda_3} \frac{\partial W}{\partial \ln \lambda_i^e} \quad (2)$$

$$\mu = \frac{\partial W}{\partial C} - \lambda_1 \lambda_2 \lambda_3 \sigma_h \frac{3}{\lambda^c} \frac{d\lambda^c}{dC} \quad (3)$$

where W is the nominal free energy density of the system, and the $\sigma_h = \frac{1}{3}(\sigma_1 + \sigma_2 + \sigma_3)$ is the hydrostatic stress. The chemical part of the energy density W_c is given by the following

$$W_c = RTC_{\max} \left(\bar{C} \ln \bar{C} + (1 - \bar{C}) \ln (1 - \bar{C}) \right) \quad (4)$$

where C_{\max} is the maximum Li concentration and the $\bar{C} = C/C_{\max}$ is the normalized nominal Li concentration in silicon, RT is the product of gas constant R and absolute temperature T . The numerical simulation, which was based on this theory, was realized using ABAQUS user-defined subroutines, the details of the coupled large deformation

simulation could be found in the Supplementary information and our previous work [37,45,46].

The geometric model and finite element mesh was shown in Fig. 3a, the length and width of the model is 40 μm , the size of the crack is the same with its size in experiments. The initial concentration \bar{C}_0 inner the electrodes was set as 0.5, and the 0.15% strain was loaded to the electrode. The parameters used during the simulation could be found in Table S1, the boundary conditions and load mode was shown in Fig. S3. Fig. 3b–f show the Li concentration \bar{C} and stress σ_{xx} evolution of the electrode over the dimensionless time t , as the model is symmetric, the concentration field and stress field at the same time were shown on the top and bottom part of each figures, respectively. During the loading process (Fig. 3c–d), the stress concentration appeared at the crack tip, and the Li was also gathering under the drive of the stress gradient. However, the Li redistribution continuously proceeds during the rest process (Fig. 3d–f), even the displacement load was constant. The concentration around crack tip was still increasing, and the affect region was also enlarging as the rest time goes on. Besides, the obvious stress relaxation around the crack tip was accrued as the increased lithiated expansion around the crack tip, which was due to the continuously Li gathering.

Fig. 4 also shows the stress and Li concentration evolution at the crack tip, the fully coupled results were contrasted with the one-way coupling results, which means the stress would not influence the electrochemical process. On the one hand, Fig. 4a–b show the remarkable difference between them, the Li concentration of the crack tip increased about 20% compared to the average concentration of the all coupled model, which was due to the stress concentration. On the other hand, the stress around crack was also decreased due to the Li gathering in return, and this interaction effect would tend to stable as the rest time goes on. Fig. 4c shows the concentrated effect of the Li distribution along the red line front the crack, and Fig. 4d directly shows reason, which is the gathering Li flux from the other area of the electrode to the crack tip. The size of Li distribution area around the crack tip is also around 5–10 μm , and it is consistent with the experimental result. The accurate analytical solution of the size effect is unobtainable due

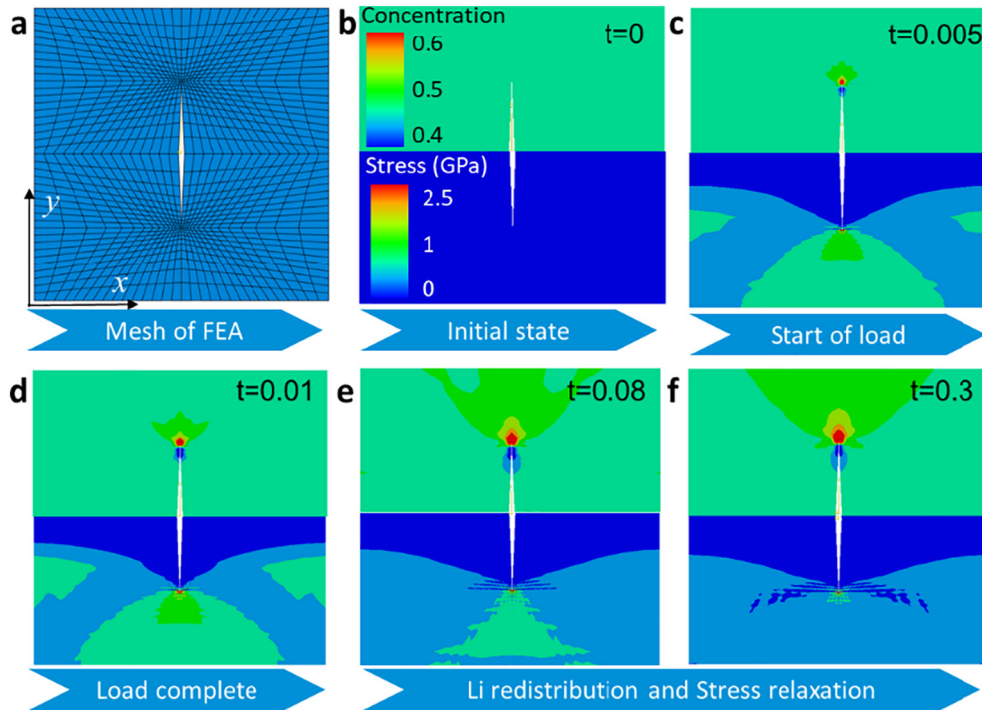


Fig. 3. (a) The geometrical model and the mesh of the FEA model. (b–f) The concentration (top part) and the stress (bottom part) evolution around the crack tip.

to the complicated boundary conditions and large chemical mechanical coupled deformation process around the crack tip. However, in consideration of the fracture mechanics [47], if the crack length and the load stress (related to the depth of delithiation) increase, the size of the Li distribution area would simultaneously be enlarged.

In summary, the Li redistribution phenomenon around the crack tip due to the coupling effect of stress and the electrochemical process was revealed by the experiments, which combining the in-situ crack monitoring and ex-situ Li concentration measurement. The results show the obviously Li concentrated behaviors around the crack tip after the

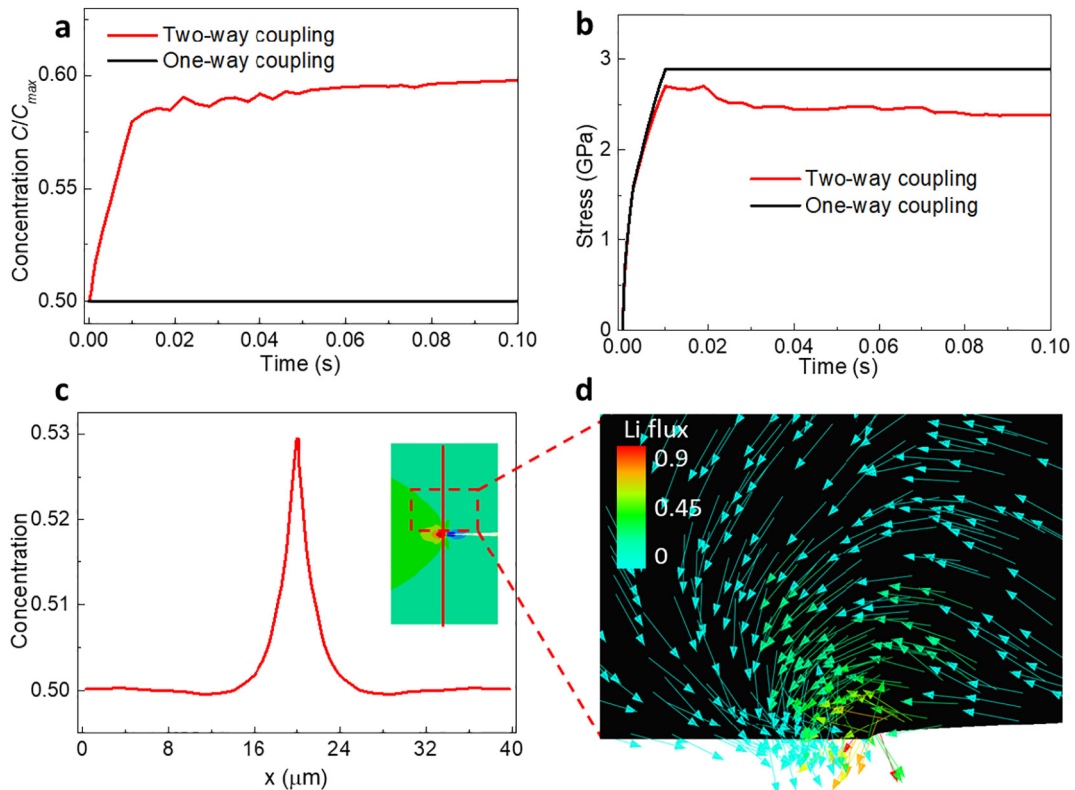


Fig. 4. (a–b) The Li concentration and stress evolution at the crack tip of the two models, respectively. (c) Li distribution along the red line front the crack tip. (d) Li flux around the crack tip at $t = 0.01$, the color of the arrow represents the value of the dimensionless Li flux. (For interpretation of the references to color in this figure legend, the reader is referred to the web version of this article.)

tensile stress load. Subsequently, the fully coupled finite element method was used to simulate the whole process of the interaction between the stress and the Li diffusion. The results clearly show the gathering Li flux around the crack tip which was consistent with the experiment results, and also reveal the mechanism of the corresponding stress relaxation. Besides, the fracture mechanism shows the size of the Li redistribution area around the crack tip is mainly influenced by the load stress and the crack length. Finally, fully understanding of the coupling effect would be useful for the design of the stable LIBs with high capacity and high volume expansion electrodes.

Financial support from National Natural Science Foundation of China (Grant Nos. 11672341 and 11572002), National Key Research and Development Program of China (Grant No. 2018YFB0104400), Innovative Research Groups of the National Natural Science Foundation of China (Grant No. 11521202), National Materials Genome Project (Grant No. 2016YFB0700600) and Beijing Natural Science Foundation (Grant Nos. 16L00001 and 2182065) is gratefully acknowledged.

Appendix A. Supplementary data

Supplementary data to this article can be found online at <https://doi.org/10.1016/j.scriptamat.2019.03.033>.

References

- [1] M. Armand, J.M. Tarascon, *Nature* 451 (2008) 652–657.
- [2] B. Dunn, H. Kamath, J.M. Tarascon, *Science* 334 (2011) 928–935.
- [3] B. Scrosati, J. Garche, *J. Power Sources* 195 (2010) 2419–2430.
- [4] D. Larcher, J. Tarascon, *Nat. Chem.* 7 (2015) 19–29.
- [5] M.R. Palacin, A. de Guibert, *Science* 351 (2016), 1253292.
- [6] K. Zhao, Y. Cui, *Extreme Mech. Lett.* 9 (2016) 347–352.
- [7] R. Xu, K. Zhao, *J. Electrochem. Energy* 13 (2016), 30803.
- [8] Y. Jin, B. Zhu, Z. Lu, N. Liu, J. Zhu, *Adv. Energy Mater.* 7 (2017) 1700715.
- [9] F. Fan, H. Yang, Z. Zeng, *Scr. Mater.* 152 (2018) 74–78.
- [10] J. Ma, J. Sung, J. Hong, S. Chae, S. Choi, G. Nam, Y. Son, S.Y. Kim, M. Ko, *J. Cho. Nat. Commun.* 10 (2019) 475.
- [11] K.W. Noh, S.J. Dillon, *Scr. Mater.* 69 (2013) 658–661.
- [12] C. Chen, T. Sano, T. Tsuda, K. Ui, Y. Oshima, M. Yamagata, M. Ishikawa, M. Haruta, T. Doi, M. Inaba, S. Kuwabata, *Sci. Rep.-UK* 6 (2016), 36153.
- [13] P. Yan, J. Zheng, T. Chen, L. Luo, Y. Jiang, K. Wang, M. Sui, J. Zhang, S. Zhang, C. Wang, *Nat. Commun.* 9 (2018) 2437.
- [14] O.O. Taiwo, J.M. Paz-Garcia, S.A. Hall, T.M.M. Heenan, D.P. Finegan, R. Mokso, P. Villanueva-Perez, A. Patera, D.J.L. Brett, P.R. Shearing, *J. Power Sources* 342 (2017) 904–912.
- [15] J. Wang, C. Eng, Y.K. Chen-Wiegart, J. Wang, *Nat. Commun.* 6 (2015) 7496.
- [16] J. Li, A.K. Dozier, Y. Li, F. Yang, Y. Cheng, *J. Electrochem. Soc.* 158 (2011) A689–A694.
- [17] X.H. Liu, L. Zhong, S. Huang, S.X. Mao, T. Zhu, J.Y. Huang, *ACS Nano* 6 (2012) 1522–1531.
- [18] I. Ryu, J.W. Choi, Y. Cui, W.D. Nix, *J. Mech. Phys. Solids* 59 (2011) 1717–1730.
- [19] H. Kim, M. Seo, M. Park, J. Cho, *Angew. Chem. Int. Ed.* 49 (2010) 2146–2149.
- [20] S.K. Soni, B.W. Sheldon, X. Xiao, A. Tokranov, *Scr. Mater.* 64 (2011) 307–310.
- [21] L. Luo, J. Wu, J. Luo, J. Huang, V.P. Dravid, *Sci. Rep.-UK* 4 (2014) 4322.
- [22] M.T. McDowell, I. Ryu, S.W. Lee, C. Wang, W.D. Nix, Y. Cui, *Adv. Mater.* 24 (2012) 6034–6041.
- [23] M. Gu, H. Yang, D.E. Perea, J. Zhang, S. Zhang, C. Wang, *Nano Lett.* 14 (2014) 4622–4627.
- [24] L. Luo, P. Zhao, H. Yang, B. Liu, J. Zhang, Y. Cui, G. Yu, S. Zhang, C. Wang, *Nano Lett.* 15 (2015) 7016–7022.
- [25] S. Kim, S.J. Choi, K. Zhao, H. Yang, G. Gobbi, S. Zhang, J. Li, *Nat. Commun.* 7 (2016), 10146.
- [26] Y.F. Gao, M. Zhou, *J. Power Sources* 230 (2013) 176–193.
- [27] H. Haftbaradaran, J. Qu, *J. Mech. Phys. Solids* 71 (2014) 1–14.
- [28] M. Zhang, J. Qu, J.R. Rice, *J. Mech. Phys. Solids* 107 (2017) 525–541.
- [29] P. Yu, H. Wang, J. Chen, S. Shen, *J. Mech. Phys. Solids* 104 (2017) 57–70.
- [30] P. Yu, J. Chen, H. Wang, X. Liang, S. Shen, *Int. J. Solids Struct.* 147 (2018) 20–28.
- [31] M. Klinsmann, D. Rosato, M. Kamlah, R.M. McMeeking, *J. Mech. Phys. Solids* 92 (2016) 313–344.
- [32] M. Klinsmann, D. Rosato, M. Kamlah, R.M. McMeeking, *J. Electrochem. Soc.* 163 (2016) A102–A118.
- [33] X. Zhang, A. Krischok, C. Linder, *Comput. Methods Appl. Mech. Eng.* 312 (2016) 51–77.
- [34] C. Miehe, H. Dal, L.M. Schänzel, A. Raina, *Int. J. Numer. Methods Eng.* 106 (2016) 683–711.
- [35] J. Réthoré, H. Zheng, H. Li, J. Li, K.E. Aifantis, *J. Power Sources* 400 (2018) 383–391.
- [36] R. Xu, K. Zhao, *J. Mech. Phys. Solids* 121 (2018) 258–280.
- [37] L. Yang, H. Chen, H. Jiang, Y. Wei, W. Song, D. Fang, *Chem. Commun. (Camb.)* 54 (2018) 3997–4000.
- [38] L. Yang, H. Chen, W. Song, D. Fang, *J. Power Sources* 405 (2018) 101–105.
- [39] X. Zhang, W. Song, Z. Liu, H. Chen, T. Li, Y. Wei, D. Fang, *J. Mater. Chem. A* 5 (2017) 12793–12802.
- [40] X. Wang, F. Fan, J. Wang, H. Wang, S. Tao, A. Yang, Y. Liu, H. Beng Chew, S.X. Mao, T. Zhu, S. Xia, *Nat. Commun.* 6 (2015) 8417.
- [41] J. Wen, Y. Wei, Y. Cheng, *J. Mech. Phys. Solids* 116 (2018) 403–415.
- [42] M. Pharr, Z. Suo, J.J. Vlassak, *Nano Lett.* 13 (2013) 5570–5577.
- [43] L.Y. Beaulieu, V.K. Cumyn, K.W. Eberman, L.J. Krause, J.R. Dahn, *Rev. Sci. Instrum.* 72 (2001) 3313–3319.
- [44] L.Y. Beaulieu, K.W. Eberman, R.L. Turner, L.J. Krause, J.R. Dahn, *Electrochem. Solid-State Lett.* 4 (2001) A137–A140.
- [45] Y. An, H. Jiang, *Model. Simul. Mater. Sci. Eng.* 21 (2013), 74007.
- [46] X. Wang, S.S. Singh, T. Ma, C. Lv, N. Chawla, H. Jiang, *Chem. Mater.* 29 (2017) 5831–5840.
- [47] H. Tada, P.C. Paris, G.R. Irwin, *The Stress Analysis of Cracks Handbook*, Third edition The American Society of Mechanical Engineers, 2000.